Pergamon

Int. J. Heat Mass Transfer. Vol. 41, No. 2, pp. 435–445, 1998

Printed in Great Britain
0017–9310/98 $19.00+0.00

PII: S0017-9310(97)00139-7

An experimental study of heat transfer and particle deposition during the outside vapor deposition process

JAEGEOL CHO, JAEYUN KIM† and MANSOO CHOI‡

Department of Mechanical Engineering, Seoul National University, Seoul, 151–742, Korea

(*Received* 28 *February* 1997)

Abstract—An experimental study has been carried out for heat transfer and particle deposition during the outside vapor deposition process. The surface temperatures of deposited layers, and rates, efficiencies and porosities of particle deposition were measured. For the characterization of the burner used, temperature distributions in the flame were measured using thermocouples and the evolution of the particle sizes was obtained using a thermophoretic sampling technique and TEM (transmission electron microscope). Of particular interest are the effects of the traversing speed of the burner, the flow rate of the chemical, and different passes of burner traverse. It is shown that the axial variation of the surface temperature can be assumed to be quasi-steady in the moving frame with the burner. As the traversing speed of burner is increased, the deposition rate, the efficiency and the porosity increase due to the decrease of surface temperatures. As the flow rate of the chemicals is increased, both the thickness of deposition layers and the surface temperature increase. Deposition rate also increases, however, deposition efficiency decreases for tests done. Later passes in the early deposition stage result in higher surface temperatures due to larger thickness of porous deposited layers, which cause the deposition rate, efficiency and porosity to decrease.

INTRODUCTION

The outside vapor deposition (OVD) process is currently utilized to manufacture high quality optical fibers. In the process shown in Fig. 1, fuel gases (H_2 and O_2), shield gas (N_2 or Ar) and carrier gas with chemical reagents such as $SiCl_4$, $GeCl_4$, etc. are injected vertically from the burner which traverses repeatedly in the axial direction under the rotating target rod. Due to the combustion of hydrogen and oxygen, the flame hydrolysis and oxidation of chemical reagents occur near the burner exit to form fine particles such as SiO_2, GeO_2, etc. The particles flow with hot gases and finally deposit on the target rod. The burner traverses repeatedly to form many deposited layers that have a desired refractive index profile by controlling the amount of dopants. When the deposition is completed, the target rod is removed and the porous hollow cylindrical deposit is dried and sintered in a furnace at high temperatures. The dehydration and sintering processes make the porous deposit become a transparent rod called a preform of optical fiber and then the drawing process produces a long thin fiber. The quality and production rate of optical fibers largely depend on the deposition process in which the understanding of heat transfer and particle transport is important since the major mechanism for particle deposition in the process is thermophoresis [1].

Most of the previous modelings of the deposition process considered thermophoretic particle deposition on a cylinder or a flat plate. Homsy *et al.* [2] and Batchelor and Shen [3] studied thermophoretic deposition on a cylinder utilizing the Blasius series solution. Garg and Jayaraj [4] calculated particle deposition on a cylinder specifying the pressure gradient of the external flow, while Alam *et al.* [5] considered a flat plate in a plane jet flow. Kang and Greif [6, 7] considered a jet flow instead of a uniform flow and calculated temperature, flow fields, and particle deposition by a numerical method using non-orthogonal curvilinear coordinates. Choi *et al.* [8] studied the effects of the deposited layers and the speed of traversing burner using a modeling which included the conduction in the porous deposited layers. In the previous modelings except Choi *et al.* [8], surface temperatures of the cylinder was assumed to be given and the effect of burner traversing speed was not considered. An experimental study has been reported by Bautista *et al.* [9] who measured the particle deposition efficiency for different target diameters and compared their results with calculations. Graham and Alam [10] carried out experiments using a stationary burner and a rotating target rod. They reported the particle deposition efficiencies for different burner-

† Korea Institute of Machinery and Materials.
‡ Author to whom correspondence should be addressed.

NOMENCLATURE

K	thermophoretic coefficient	x	axial coordinate measured from the burner starting position
M_{SiCl_4}	molecular weight of $SiCl_4$	z	height above burner exit.
M_{SiO_2}	molecular weight of SiO_2		
T	temperature	Greek symbol	
V_{burner}	traversing speed of burner	ν	kinematic viscosity.
V_T	thermophoretic velocity		

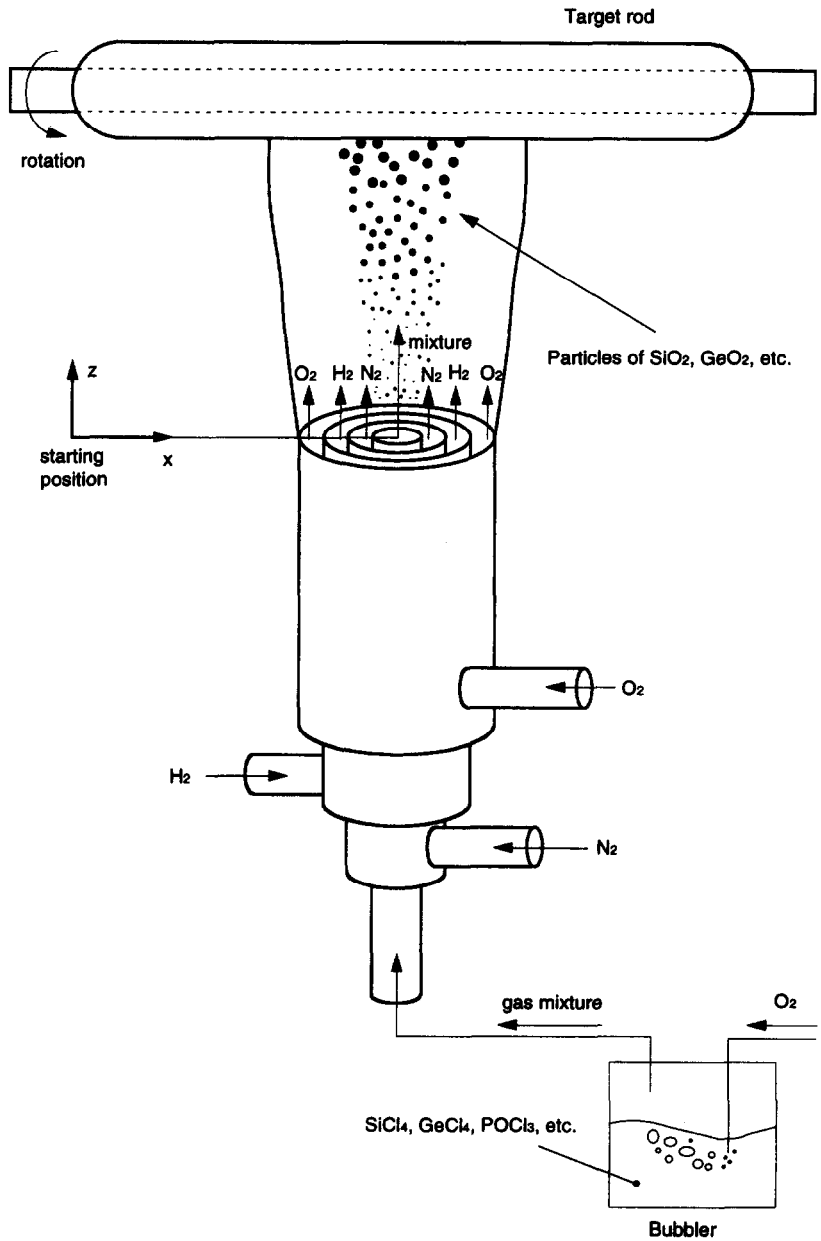

Fig. 1. Schematic of OVD deposition process.

target distances and carrier gas flow rates. Hwang and Daily [11] experimentally studied electric field-enhanced deposition on a disk and Kim [12] studied the particle deposition on a cylinder using TiO_2 particles.

The previous experimental studies on the OVD process were relatively small and the scopes studied previously were rather limited. In particular, the effects of the traversing speed of burner and the different passes of deposition on the surface temperature and particle deposition (rate, efficiency and porosity of deposition) have not been reported. In this study, the effects of burner speed, different passes and carrier gas flow rates on particle deposition have been studied. The flame temperatures were measured and the morphology of particles was also obtained using a thermophoretic sampling technique [13].

The objectives of the present study are to establish further experimental data for the heat transfer and particle deposition in the process and to investigate the effects of the important process parameters such as the burner speed, different passes, and carrier gas flow rate.

EXPERIMENTAL APPARATUS AND PROCEDURE

The schematic of the experimental apparatus is shown in Fig. 2(a). A stepping motor driven traverse system has been constructed using a PC based pulse algorithm to control the speed of traversing burner, and the target rod is rotated by AC motor. Carrier gas O_2 passes through liquid $SiCl_4$ in a bubbler to vaporize $SiCl_4$ and then the mixture flows into the burner. The flow rate of the carrier gas O_2, fuel gases (H_2, O_2), and shield gas N_2 are measured with the rotameters that were calibrated using a wet test gas-meter. The exit of the burner is composed of a series of concentric annuli from which the mixture of $SiCl_4$ and O_2, N_2, H_2 and O_2 are injected [refer to Fig. 2(b) for a detailed configuration]. The shield gas prevents undesirable particle deposition on the center nozzle where the $SiCl_4$ vapor is injected, but large amounts of a shield gas can diminish the particle deposition efficiency by lowering the flame temperature. In this study, the burner was designed to lower the center nozzle below the other concentric nozzles from which fuels are released, and by using a movable joint, the spacing between the center nozzle and the other surrounding nozzles can be controlled to minimize the particle deposition on the center nozzle. This configuration successfully prevented particle deposition around the $SiCl_4$ nozzle with only small amount of a shield gas due to the decreased temperatures near the surface of the center nozzle that is positioned apart from the flame location.

B type (Pt/6%Rh–Pt/30%Rh) thermocouples were used to measure the flame temperature of the burner and the data were transferred to PC via A/D converter. The measurements were performed three times for each condition and the mean values were used to obtain final flame temperature distributions.

In this study, an alumina rod (diameter = 19.05 mm, length = 920 mm) and $SiCl_4$ were used as a target rod and chemical reagent, respectively. The distance between the burner exit and the center of the rod is 34 mm, and the rod rotates at 90 rpm. The burner moves at a constant speed ranging from 5 to 20 cm min^{-1} and returns at the speed of about 300 cm min^{-1} to repeat the pass when it reaches the location 650 mm away from the starting position. While the burner returns, the oxygen lines connected to both the burner and the bubbler are closed. The fuel gas flow rates are 5.8 l min^{-1} for H_2 and 7.3 l min^{-1} for O_2 (equivalence ratio = 0.4). The flow rate of N_2 as a shield gas is 1 l min^{-1}, and the flow rates of carrier gas O_2 are varied from 0.3 to 0.7 l min^{-1}. During the tests, following reactions of SiO_2 particle formation occur

$$SiCl_4(g) + O_2(g) \rightarrow SiO_2(s) + 2Cl_2(g)$$

$$SiCl_4(g) + 2H_2O(g) \rightarrow SiO_2(s) + 4HCl(g)$$

where (g) and (s) indicate gas and solid, respectively.

The particles formed move with hot gases in the flame and are deposited on the rotating target rod due to thermophoresis. A thermophoretic sampling technique and TEM measurement [13] were employed for a morphological description of evolution of flame-generated particles.

The surface temperatures of the deposited layers were measured with two infrared thermometers. The one (IRCON, Series 7000-799C10) for temperatures greater than 1000°C has a focal length 330 mm, spectral response 4.8–5.2 μm and target diameter 3.3 mm; and the other (MINOLTA, TA-0510) for temperatures below 1000°C has a focal length 500 mm, spectral response 8–13 μm and target diameter 9 mm. To estimate the emissivity of the deposited layers, a B type thermocouple was installed on the surface of the deposited layer and then the surface temperatures were measured by using both infrared thermometers and the thermocouple under the condition of non-rotating target rod heated by moving burner. From the comparison of two measurements, the emissivity of the deposited layer was determined to be 1.0 for the infrared thermometer having the spectral range from 8 to 13 μm, but for the infrared thermometer to measure temperatures higher than 1000°C (spectral response 4.8–5.2 μm), the emissivity was found to vary with the porosities of the layers. Therefore, when the surface temperature exceeds 1000°C, each case of different deposition conditions was tested under the condition of non-rotating target rod to determine emissivity and the resulting different emissivities were used in the determination of surface temperatures for the rotating deposited rod. The variation of surface temperatures in the circumferential direction was neglected due to the rotation of the rod with 90 rpm [8].

The mass flow rate of $SiCl_4$ has been determined by measuring the weight change of the bubbler for a

(a)

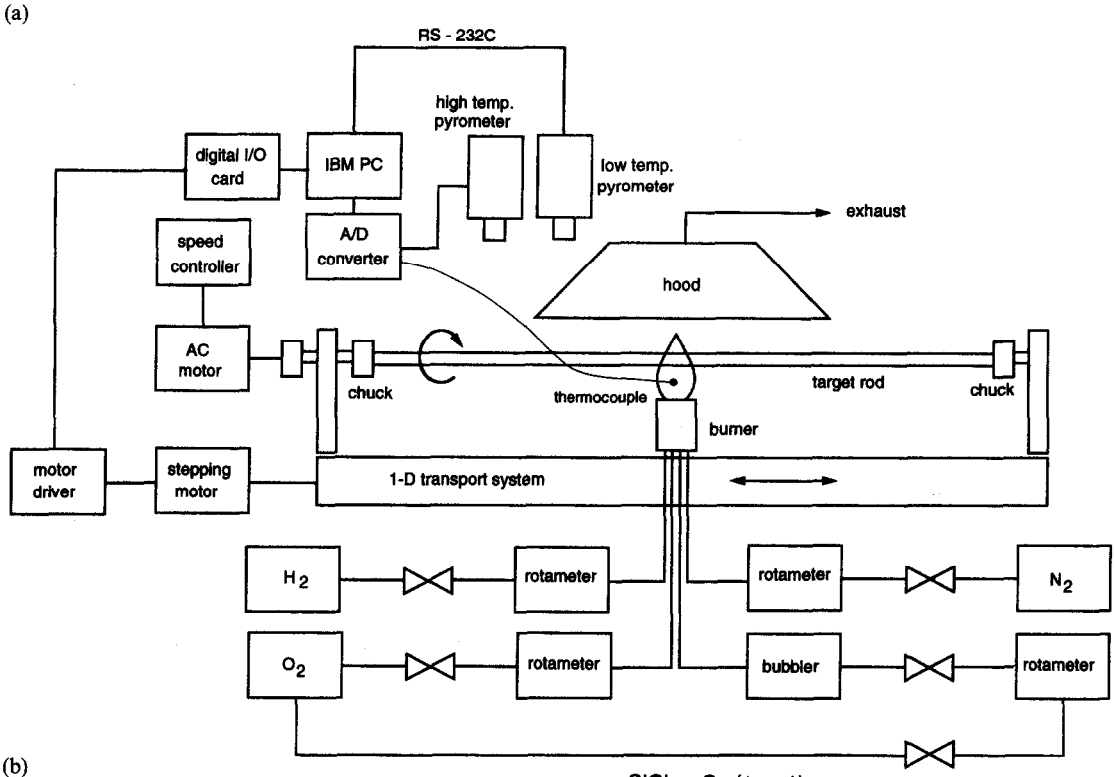

(b)

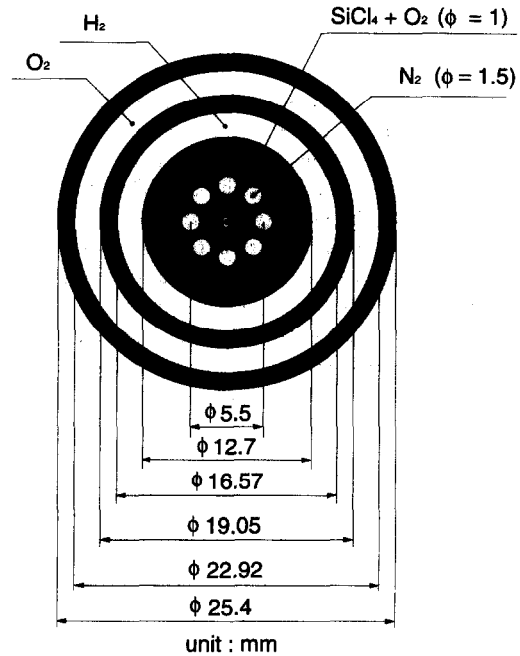

Fig. 2. (a) Schematic diagram of the experimental apparatus for deposition process; (b) burner exit geometry.

given time interval using an electronic balance. From the mass flow rate of $SiCl_4$, the maximum amount of SiO_2 formed can be determined. The comparison of this with the actual deposited mass of SiO_2 yields the overall efficiency of particle deposition. The deposition rate of SiO_2 is determined from the difference in weight between the original rod and the deposited one in a given time interval. The rate and efficiency of particle deposition are obtained from the following relations.

particle deposition rate

= deposited SiO_2 mass/deposition time
= weight change of the rod/(burner traversing distance/burner speed)

particle deposition efficiency
= deposited SiO_2 mass/maximum possible formation of SiO_2
= (weight change of the rod/M_{SiO_2})/(weight change of the bubbler/M_{SiCl_4})

where M_{SiO_2} and M_{SiCl_4} are molecular weights of SiO_2 and $SiCl_4$, respectively.

Porosities of the deposited layers which may affect the subsequent processes of drying and sintering were determined from the ratio of the density of deposited layers to that of a fused silica. The volume of the deposited layer was obtained from the burner traversing distance and the target rod diameters measured before and after deposition. Dividing the deposited SiO_2 mass by the volume gives the average density of the deposited layers, which is then used for the determination of porosity. The diameter of the rod was measured at four different locations using a cathetometer (MARUBISHI, PRM-5) with 0.01 mm accuracy.

An uncertainty analysis was performed for the measured values of the flame temperature, surface temperature of the deposited layers, deposition rate, deposition efficiency and porosity following the procedure described in Benedict [14]. For the flame temperatures, the average relative uncertainty by random error is 6.3%. The relative uncertainties of deposition rate, efficiency and porosity are estimated to be 11.7, 4.5 and 2.9%, respectively, for given conditions (V_{burner} = 10 cm min^{-1}, carrier gas flow rate = 0.5 l min^{-1}, 4 passes). The mass flow rate of $SiCl_4$ has the largest uncertainty (14.5%) caused by even small temperature change of the bubbler during the experiments and by the use of rotameters to measure the carrier gas flow rate. This resulted in a large random error in the particle deposition rate. For the above deposition conditions, the relative uncertainty of the maximum surface temperature in the fourth pass was 6.7%.

RESULTS AND DISCUSSION

The dominant particle deposition mechanism in the OVD process is thermophoresis; that is, from the net force that a suspended particle experiences in the direction of decreasing temperature in a non-isothermal medium, and the thermophoretic velocity is expressed as the following [15].

$$\vec{V}_T = -\frac{Kv}{T}\nabla T.$$

Therefore, the determination of temperature fields around the target rod is important. In particular, since the growth of the SiO_2 particles is strongly influenced by its viscosity which is dependent on temperature [16], the determination of the flame temperature is needed for the characterization of the burner and for the modeling of the OVD process. For the burner used, the oxy-hydrogen flame temperatures were measured in the absence of SiO_2 particles. The temperature indicated by the thermocouple immersed in a flame is lower than the real gas temperature due to the radiation heat loss of the thermocouple bead. Neglecting the error induced by the conduction through the lead wire and the effect of disturbance in the flame by the insertion of a thermocouple probe, an energy balance equation can be made such that the heat convected from the hot gas stream to the bead is equal to the radiation heat loss of the bead [17]. The calibrated flame temperatures were calculated from the energy balance.

Figure 3 shows the flame temperature distributions in the radial direction for the case without a shield gas. The flame temperatures decrease with height and the distributions become less flat. The shield gas has an important effect on flame temperatures, which is shown in Fig. 4. The temperatures of the center region near the burner exit are significantly decreased because the inert gas N_2 prevents the diffusion of the hot gas produced by the combustion of H_2 and O_2 to the center region of the burner. At higher locations from the burner exit, the profiles become similar to those of Fig. 3, but the overall temperatures have been decreased.

The measurements of surface temperatures of the deposited layers are based on the assumption that the axial temperature distribution is steady with respect to the coordinate moving with the burner; that is, the temperatures depend only on the relative distances from the burner. To validate this quasi-steady assumption, transient temperatures at different locations have been measured as the burner traverses. Figure 5(a) shows transient surface temperatures along the rod at five different locations as a function of the position of burner which is equivalent to the elapsed time after the torch movement. A sharp temperature rise was observed near the measuring location when the burner passed the location. In Fig. 5(b), these transient data measured at five different axial locations are plotted using the coordinate moving with the burner. These data now seem to fit on one curve, which supports the quasi-steady assumption used in this study.

The effect of the burner traversing speed on surface temperatures for first pass is shown in Fig. 6. As the speed is increased, surface temperatures decrease because of the reduction of the time needed for the burner to heat the rod. The decrease in porous (insulating) silica layer thickness has been observed for higher burner speeds and this may be another factor to have lower surface temperatures. Choi *et al.* [8] showed the insulation effect of the porous deposited silica layer resulted in higher surface temperatures for larger thicknesses up to 5 mm. Figure 7 shows the surface temperature distributions of fourth pass for three different burner speeds of 5, 10 and 15 cm min^{-1} where the emissivities for the pyrometer used for temperature measurements greater than 1000°C were found to be 0.45, 0.4 and 0.35, respectively. It is noted

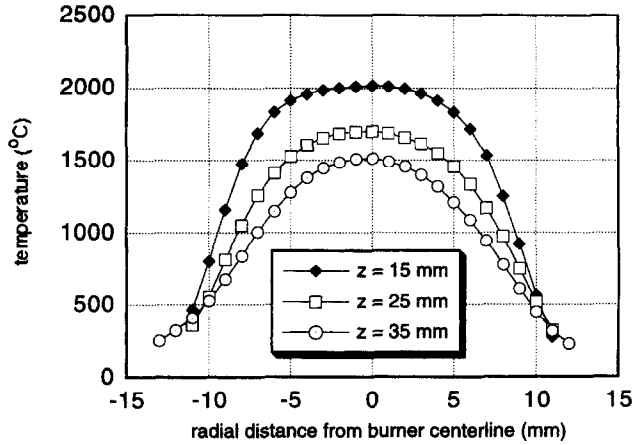

Fig. 3. Flame temperature distributions without N_2 (H_2 = 3.5 l min^{-1}, O_2 = 12 l min^{-1}, N_2 = 0 l min^{-1}, no carrier gas).

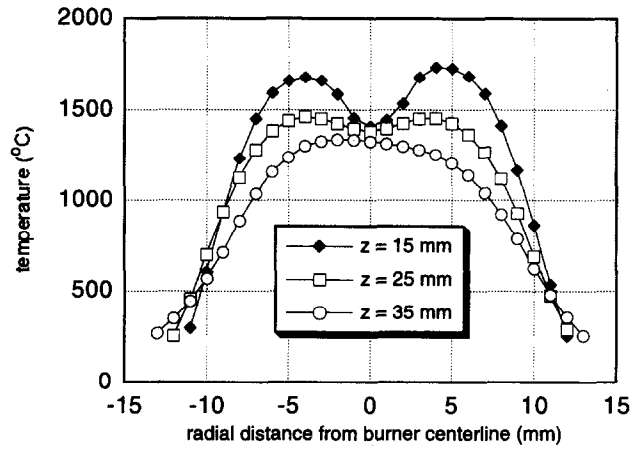

Fig. 4. Flame temperature distributions with N_2 (H_2 = 3.5 l min^{-1}, O_2 = 12 l min^{-1}, N_2 = 2 l min^{-1}, no carrier gas).

that these emissivities were obtained by comparing the infrared thermometer measurements with the thermocouple measurements under the non-rotating condition. The curves are similar to those of Fig. 6, but the differences between the maximum temperatures have become smaller for later passes. Since the decrease in surface temperatures enhance thermophoresis by increasing temperature gradients near the surface, it is thought that the particle deposition efficiencies would be larger for higher burner speeds. This is confirmed in Fig. 8 where the efficiency, the rate and the porosity of deposition are shown. As the burner speed is increased, the efficiency increases, which means the increase of deposition rate for the same feed rate of $SiCl_4$. This is consistent with the numerical results of Choi *et al.* [8]. Figure 8 also shows the increase of porosities of the deposited layers for higher burner speeds due to the reduced surface temperatures.

Figure 9 shows the effect of carrier gas O_2 flow rates which is equivalent to the effect of the flow rates of $SiCl_4$, on the surface temperatures. The surface temperatures are greatly influenced by the presence of deposited SiO_2 layers because of the large difference of thermal conductivities between the original target rod and the porous deposited layers [8]. When the alumina target rod is heated by the moving burner without deposition, surface temperatures become low due to the relatively high thermal conductivity of the rod (see triangles in Fig. 9). Once the deposition occurs, the low conductivity of the deposited layers cause the surface temperatures to increase. As the carrier gas flow rate is increased, the deposition thickness increases, which causes surface temperatures to increase due to the increasing insulation effect of deposited layers. The effect of carrier gas flow rates on deposition efficiencies, rates, and porosities for four passes are shown in Fig. 10. As the flow rate increases, increasing surface temperatures decrease the efficiency, but the deposition rate increases since the feed rate of $SiCl_4$ is increased. If the flow rate is further increased, reduced flame residence time owing to the increased injection velocity of $SiCl_4$ may cause incomplete reactions of $SiCl_4$, which also would lower deposition efficiency. The porosities are relatively insensitive to the flow rates. It seems that on the

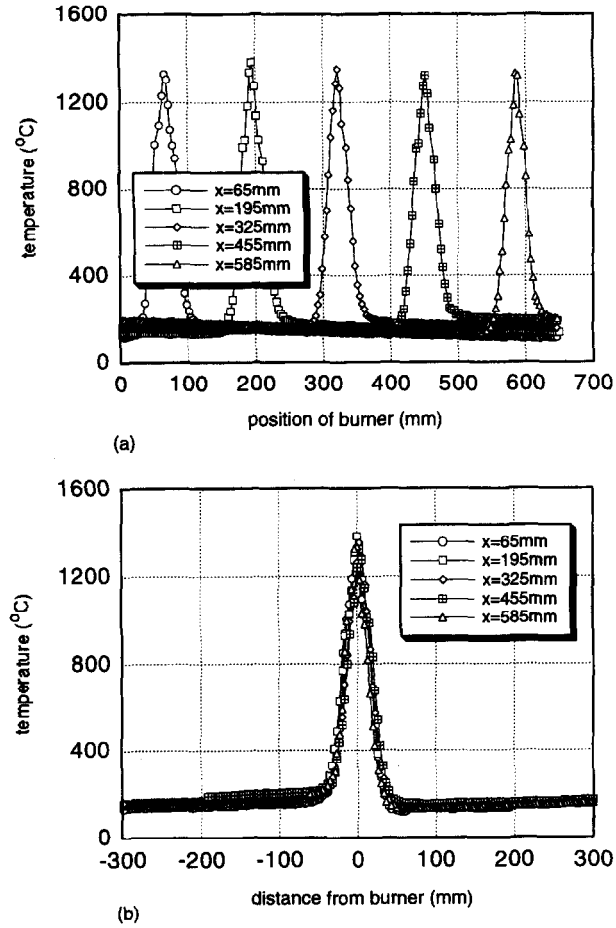

Fig. 5. (a) Transient variations of surface temperatures for different axial locations; (b) variations of surface temperatures for different axial locations in moving coordinate (V_{burner} = 10 cm min^{-1}, carrier gas O_2 = 0.5 l min^{-1}, 4th pass).

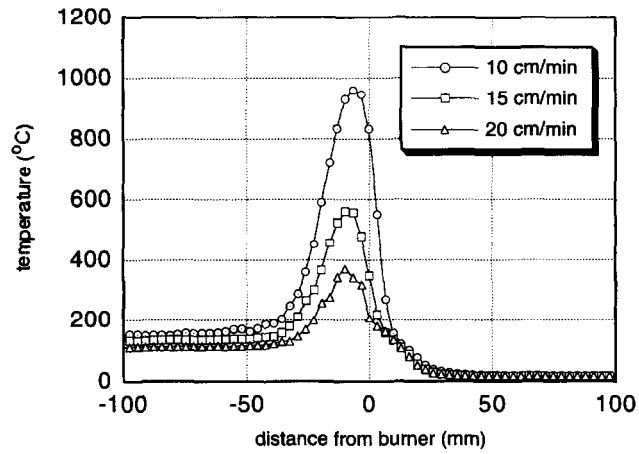

Fig. 6. Effect of burner speed on surface temperature distributions (carrier gas O_2 = 0.5 l min^{-1}, 1st pass).

determination of porosity the effect of reducing flame residence time cancels the effect of increasing surface temperatures for high flow rates. Particle residence time in a flame determines particle sizes and shapes, which would affect the porosity of deposited layer. Different surface temperatures measured for different flow rates will also affect the porosity of deposition. This will be discussed again in Figs. 13(e)–(g), in which the shape of particles collected at the same heights for different carrier gas flow rates are shown.

Figure 11 shows the surface temperature distributions for different numbers of pass. As expected,

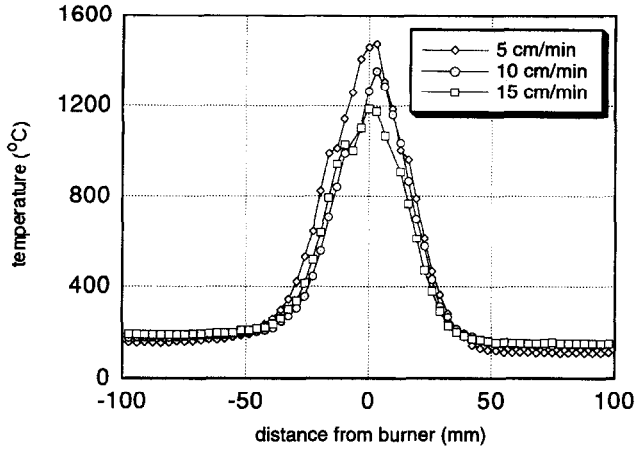

Fig. 7. Effect of burner speed on surface temperature distributions (carrier gas $O_2 = 0.5$ l min^{-1}, 4th pass)

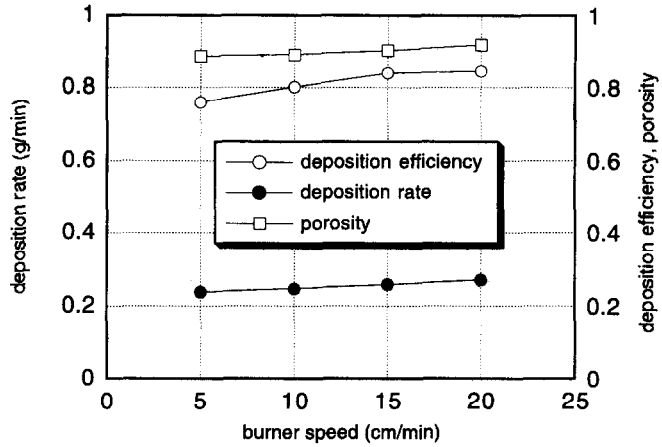

Fig. 8. Deposition efficiency, rate and porosity for different burner speeds (carrier gas $O_2 = 0.5$ l min^{-1}).

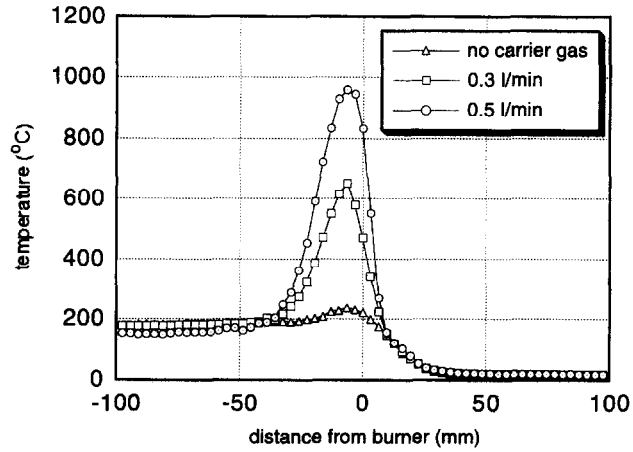

Fig. 9. Effect of carrier gas flow rate on surface temperature distributions ($V_{burner} = 10$ cm min^{-1}, 1st pass).

deposition of particles results in higher surface temperatures than for the case of heating the rod without deposition, and further passes show even higher temperatures. Figure 12 is the result of deposition for 2, 4 and 6 passes under the same conditions ($V_{burner} = 10$ cm min^{-1}, carrier gas $O_2 = 0.5$ l min^{-1}). As the pass is repeated, the average efficiency, rate and porosity decrease, which would be due to the increasing surface temperatures as evidenced by Fig. 11.

Figures 13(a)–(e) are transmission electron micrographs which show a morphological evolution of flame-generated particles collected at different heights

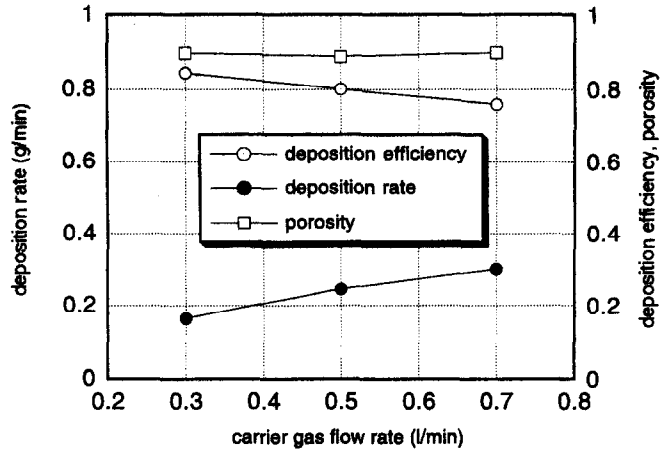

Fig. 10. Deposition efficiency, rate and porosity for different carrier gas flow rates (V_{burner} = 10 cm min^{-1}).

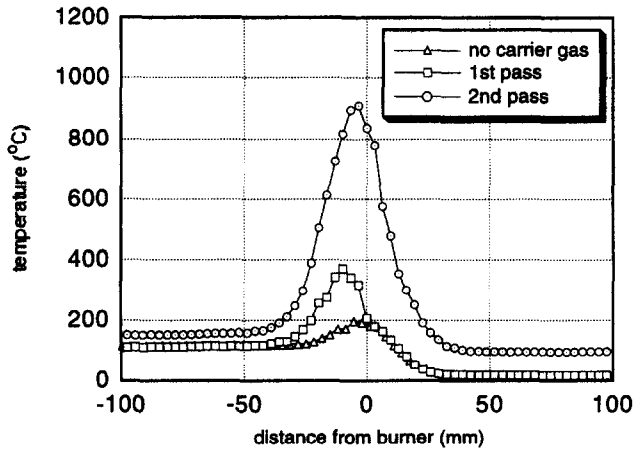

Fig. 11. Axial surface temperature distributions for different passes (V_{burner} = 20 cm min^{-1}, carrier gas O_2 = 0.5 l min^{-1}).

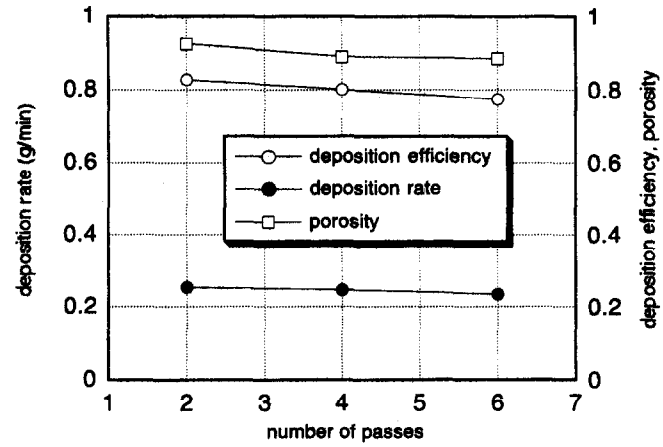

Fig. 12. Deposition efficiency, rate and porosity for different number of passes (V_{burner} = 10 cm min^{-1}, carrier gas O_2 = 0.5 l min^{-1}).

from the burner exit when the carrier gas flow rate is 0.3 l min^{-1}. Near the burner exit, chain cluster type aggregates composed of many primary particles of nearly same sizes are observed. As the particles move, they collide with each other and become larger, and sintering processes yield almost spherical shapes at

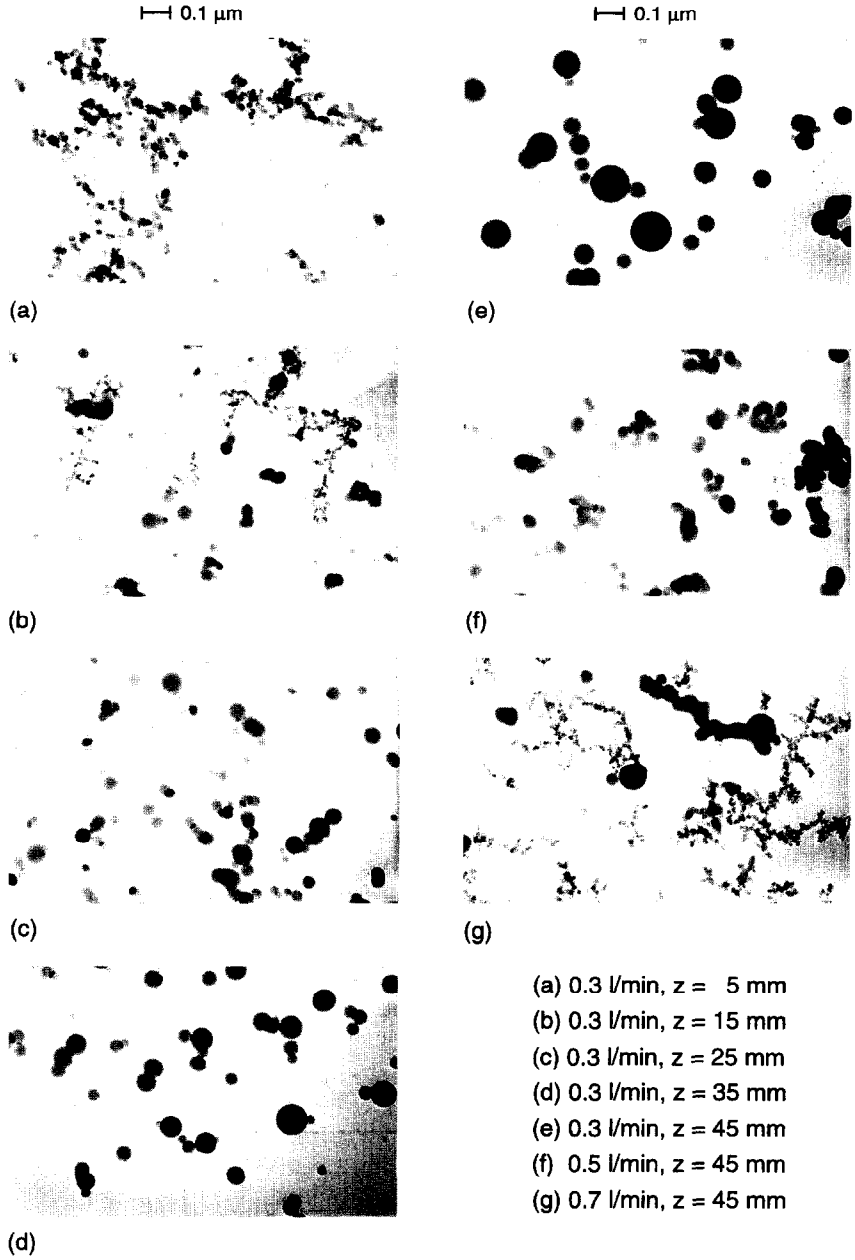

Fig. 13. TEM micrographs of silica particles collected at different heights and different carrier gas flow rates: (a) 0.3 l min^{-1}, $z = 5$ mm; (b) 0.3 l min^{-1}, $z = 15$ mm; (c) 0.3 l min^{-1}, $z = 25$ mm; (d) 0.3 l min^{-1}, $z = 35$ mm; (e) 0.3 l min^{-1}, $z = 45$ mm; (f) 0.5 l min^{-1}, $z = 45$ mm; (g) 0.7 l min^{-1}, $z = 45$ mm.

higher locations [18]. Note that the particles collected at higher locations are of different sizes and larger than those collected at lower locations. Comparing Fig. 13(e)–(g), the effect of flow rates can be identified. The case of 0.5 l min^{-1} resulted in smaller size and incomplete sintering at $z = 45$ mm [see Fig. 13(f)]. An even higher flow rate of 0.7 l min^{-1} produced both spherical particles and aggregates at the same height, which resembled the shapes in Fig. 13(b) which showed particles at lower location at $z = 15$ mm for the flow rate of 0.3 l min^{-1}. As the flow rate is increased, the average particle size is reduced and the particles deviate from spherical shapes for high flow rates at the axial distance of 45 mm. This is the result of the reduced residence time for larger flow rates. In particular, in the case of large carrier gas flow rate (0.7 l min^{-1}) the chain cluster type aggregates and large spherical particles are observed to coexist. The fact that different particle sizes and shapes evolved for different flow rates did not affect significantly the porosities of the deposited layers (see Fig. 10) indicates that partial sintering effect which depends on the resulting surface temperatures for different flow rate also contributed the determination of porosity.

CONCLUSIONS

An experimental study has been carried out for heat transfer and particle deposition during the OVD process. The effects of burner speed, carrier gas flow rate and different passes were studied and the following conclusions have been drawn.

(1) The surface temperatures of the rotating target rod can be assumed to be quasi-steady in the moving frame with the burner.

(2) As the burner speed is increased, surface temperatures decrease, which causes the deposition efficiency, rate and the porosity to increase.

(3) As the carrier gas flow rate is increased, the efficiency decreases due to the increase of surface temperatures, but the deposition rate increases. Porosities are found to be relatively insensitive to the flow rates.

(4) Later passes result in higher surface temperatures which cause the efficiency, rate and porosity to decrease.

(5) The sizes of particles rapidly increase by coagulations and aggregates of small primary particles existed near the burner exit have evolved to spherical polydisperse particles.

(6) Average particle sizes are reduced for higher carrier gas flow rates. For 0.7 l min^{-1} flow rate, spherical particles and aggregates coexist even at $z = 45$ mm.

Acknowledgements—This work was supported by the Ministry of Education, Korea, (ME93-A-13). This study was also partially supported by the Korean Ministry of Education through the research fund for advanced materials in 1996.

REFERENCES

1. Simpkins, P. G., Greenberg-Kosinski, S. and MacChesney, J. B., Thermophoresis: the mass transfer mechanism in modified chemical vapor deposition. *Journal of Applied Physics*, 1979, **50,** 5676–5681.
2. Homsy, G. M., Geyling, F. T. and Walker, K. L., Blasius series for thermophoretic deposition of small particles. *Journal of Colloid and Interface Science*, 1981, **83,** 495–501.
3. Batchelor, G. K. and Shen C., Thermophoretic deposition of particles in gas flowing over cold surfaces. *Journal of Colloid and Interface Science*, 1985, **107,** 21–37.
4. Garg, V. K. and Jayaraj, S., Thermophoretic deposition over a cylinder. *International Journal of Engineering Fluid Mechanics*, 1990, **3,** 175–196.
5. Alam, M. K., Graham, G. M., Janakiraman, V. and Greaves, J., Numerical analysis of thermophoretic transport in the OVD process. *Numerical Heat Transfer*, 1990, **130,** 67–72.
6. Kang, S. H. and Greif, F., Flow and heat transfer to a circular cylinder with a hot impinging air jet. *International Journal of Heat and Mass Transfer*, 1992, **35,** 2173–2183.
7. Kang, S. H. and Greif, R., Thermophoretic transport in the outside vapor deposition process. *International Journal of Heat and Mass Transfer*, 1993, **36,** 1007–1018.
8. Choi, M., Song, Y. and Kang, S. H., Conjugate heat transfer and particle transport in outside vapor deposition process. *Numerical Heat Transfer, Part A*, 1995, **28,** 39–54.
9. Bautista, J. R., Walker, K. L. and Atkins, R. M., Modeling heat and mass transfer in optical waveguide manufacture. *Chemical Engineering Progress*, 1990, 47–52.
10. Graham, G. M. and Alam, M. K., Experimental study of the outside vapor deposition process. *Journal of Aerosol Science and Technology*, 1991, **15,** 69–76.
11. Hwang, J. and Daily, J. W., Electric field enhanced deposition in flame synthesized materials manufacturing. *Journal of Aerosol Science*, 1995, **26,** 5–18.
12. Kim, Y. J., Particle transport and deposition from nonisothermal gas-particle flows. Ph.D. thesis, Korea Advanced Institute of Science and Technology, 1991.
13. Dobbins, R. A. and Megaridis, C. M., Morphology of flame-generated soot as determined by thermophoretic sampling. *Langmuir*, 1987, **3,** 254–250.
14. Benedict, R. P., *Fundamentals of Temperature, Pressure, and Flow Measurements*, 3rd edn. Wiley, New York, 1984, pp. 172–199.
15. Talbot, L., Cheng, R. K., Schefer, R. W. and Willis, D. R., Thermophoresis of particles in a heated boundary layer. *Journal of Fluid Mechanics*, 1990, **101,** 737–758.
16. Ulrich, G. D. and Riehl, J. W., Aggregation and growth of submicron oxide particles in flames. *Journal of Colloid and Interface Science*, 1982, **87,** 257–265.
17. Chung, S. and Katz, J. L., The counter diffusion flame burner: a new tool for the study of the nucleation of refractory compounds. *Combustion and Flame*, 1985, **61,** 271–284.
18. Chang, H. and Biswas, P., In situ light scattering dissymmetry measurements of the evolution of the aerosol size distribution in flame. *Journal of Colloid and Interface Science*, 1992, **153,** 157–166.